HAL
open science

Autofluorescence-Free In Vivo Imaging Using Polymer-Stabilized Nd 3+ -Doped YAG Nanocrystals

Alexandra Cantarano, Jingke Yao, Marija Matulionyte, José Lifante, Antonio Benayas, Dirk Ortgies, Fiorenzo Vetrone, Alain Ibanez, Corine Gerardin, Daniel Jaque, et al.

To cite this version:

Alexandra Cantarano, Jingke Yao, Marija Matulionyte, José Lifante, Antonio Benayas, et al.. Autofluorescence-Free In Vivo Imaging Using Polymer-Stabilized Nd 3+ -Doped YAG Nanocrystals. ACS Applied Materials & Interfaces, 2020, 12 (46), pp.51273-51284. 10.1021/acsami.0c15514 . hal-03099455

HAL Id: hal-03099455

https://hal.science/hal-03099455v1

Submitted on 6 Jan 2021

HAL is a multi-disciplinary open access archive for the deposit and dissemination of scientific research documents, whether they are published or not. The documents may come from teaching and research institutions in France or abroad, or from public or private research centers.

L'archive ouverte pluridisciplinaire **HAL**, est destinée au dépôt et à la diffusion de documents scientifiques de niveau recherche, publiés ou non, émanant des établissements d'enseignement et de recherche français ou étrangers, des laboratoires publics ou privés.

Autofluorescence-free *in vivo* imaging using polymer-stabilized Nd^{3+}-doped YAG nanocrystals

*Alexandra Cantarano,[1] Jingke Yao,[2] Marija Matulionyte,[3] José Lifante,[4,5] Antonio Benayas,[2,5] Dirk H. Ortgies,[2,5] Fiorenzo Vetrone,[3] Alain Ibanez,[1] Corine Gérardin,[6] Daniel Jaque, [2,5] Géraldine Dantelle[1]**

[1] Univ. Grenoble Alpes, CNRS, Grenoble INP, Institut Néel, 38000 Grenoble, France

[2] Fluorescence Imaging Group, Departamento de Física de Materiales, Universidad Autónoma de Madrid, C/ Francisco Tomás y Valiente 7, 28049 Madrid, Spain

[3] Institut National de la Recherche Scientifique, Centre Énergie, Matériaux et Télécommunications, Université du Québec, 1650 Boul. Lionel-Boulet, Varennes (Québec) J3X 1S2, Canada

[4] Fluorescence Imaging Group, Departamento de Fisiología, Facultad de Medicina, Universidad Autónoma de Madrid, Avda. Arzobispo Morcillo, 2; Madrid 28029, Spain;

[5] Nanobiology Group, Instituto Ramón y Cajal de Investigación Sanitaria IRYCIS, Ctra. Colmenar km. 9.100, 28034 Madrid, Spain

[6] ICGM, Univ. Montpellier, CNRS UMR 5253, ENSCM, 240 Avenue E. Jeanbrau, 34296 Montpellier Cedex 5, France

KEYWORDS: bio-imaging, YAG:Nd^{3+} nanoparticles, block copolymer, near-infrared fluorescence, autofluorescence removal, nanothermometry

ABSTRACT Neodymium-doped yttrium aluminum garnet (YAG:Nd^{3+}) has been widely developed during roughly the last sixty years and has been an outstanding fluorescent material. It has been considered as the gold standard among multipurpose solid-state lasers. Yet, the successful downsizing of this system into the nano regimen has been elusive, so far. Indeed, the synthesis of a garnet structure at the nanoscale, with enough crystalline quality for optical applications was found to be quite challenging. Here, we present an improved solvothermal synthesis method producing YAG:Nd^{3+} nanocrystals of remarkably good structural quality. Adequate surface functionalization using asymmetric double-hydrophilic block copolymers, constituted of a metal-binding block and a neutral water soluble block, provides stabilized YAG:Nd^{3+} nanocrystals with a long term colloidal stability in aqueous suspensions. These newly stabilized nanoprobes offer spectroscopic quality (long lifetimes, narrow emission lines, and large Stokes shift) close to that of bulk YAG:Nd^{3+}. The narrow emission lines of YAG:Nd^{3+} nanocrystals are exploited by differential infrared fluorescence imaging, thus achieving an autofluorescence-free *in vivo* readout. In addition, nanothermometry measurements, based on the ratiometric fluorescence of the stabilized YAG:Nd^{3+} nanocrystals, are demonstrated. The progress here reported paves the way for the implementation of this new stabilized YAG:Nd^{3+} system in the preclinical arena.

1. Introduction

Fluorescence-based imaging techniques are being used more frequently in biomedical research, for example in cytometry and bio-imaging.[1,2,3] This latter application allows for the visualization of cancerous cells prior to surgery, resulting in more optimal targeting of malignant cells and ultimately improving the prognosis of the patient.[4,5] The principle of bio-imaging is based on the injection of optical markers (fluorescent molecules or nanoprobes) that can be tracked *in vivo*

owing to their fluorescence properties. Fluorescent organic dyes, metallic and inorganic nanocrystals have been widely developed for this purpose.[6,7] However, their excitation and emission wavelength ranges are quite often in the visible range, i.e. where the absorption of biological tissues and hemoglobin is high and where light scattering is also strong, which significantly limits the detection of the fluorescence of markers.

For the detection of early-stage cancerous cells or for the understanding of complex biological mechanisms, it is essential to develop new fluorescent probes whose spectroscopic properties lie in the so-called biological transparency windows (BWs).[8] The design of organic dyes and quantum dots exhibiting near-infrared (NIR) fluorescence in the first BW (from 680 nm to 950 nm) has been, and still is, a very challenging task [9,10,11,12,13] as researchers face low fluorescence efficiency in the NIR range and a lack of photostability. More recently, nanoprobes with excitation and emission properties in the second BW (1000-1350 nm) have been proposed[14] and will allow for in-depth imaging and increased sensitivity as autofluorescence and light scattering are considerably lowered in this range.[15] Moreover, in the third BW situated between 1500 and 1800 nm, the absorption of biological tissues and light scattering are further reduced.

Aside from the factors explained above, background autofluorescence represents quite a challenging obstacle to overcome in the field of biomedical imaging. The background emission generated by some biological compounds complicates the visualization of the probes used as the contrast agents and lead to fluorescence images with poor signal-to-background contrast. Although different approaches are currently in use to minimize the autofluorescence, including time gating or spectral filtering,[16, 17] they are limited by the broad spectral fingerprint of the NIR probe (such as dyes and quantum dots) or suffer from a tradeoff between background removal and the intrinsic low intensity of the emitted signal. Therefore, the race is still very much on to develop new NIR

probes featuring intrinsic spectral properties, i.e. narrower emission lines, which may allow for a more complete suppression of autofluorescence in a simple and straightforward way, towards an effective filtering of the signal without paying a high toll in the process. Such spectral narrowing of emission lines should be achieved while maintaining high fluorescence brightness to ensure high contrast in fluorescence images without requiring neither high illumination intensities nor large administration doses.

In this context, rare earth doped inorganic nanocrystals, and especially neodymium (Nd^{3+})-doped nanocrystals, have emerged as very promising materials for *in vivo* bio-imaging. Indeed, when incorporated inside a matrix, Nd^{3+} presents several electronic transitions that lead to stable fluorescence in the different BWs under 800 nm excitation. An additional advantage of Nd^{3+}-doped materials is their ability to exhibit emission peaks whose intensity is temperature-dependent in the physiological temperature range.[18,19] Several types of Nd^{3+} doped nanocrystals (SrF_2,[20], LaF_3,[21] $NaGdF_4$,[22] CaF_2,[23] and $NaHoF_4$ [24]) have been indeed used for *in vivo* imaging. In a recent paper, B. Del Rosal *et al.* compared different host matrices [25] and concluded that Nd^{3+}-doped $Y_3Al_5O_{12}$ (YAG:Nd^{3+}) nanocrystals are good candidates as they can be easily excited by commercially available diodes (at 808 nm). They present narrow emission lines, which are a competitive advantage for autofluorescence removal. However, it is not an easy task to prepare YAG:Nd^{3+} nanocrystals with controlled size and high crystal quality, a strong requirement to obtain high fluorescence signal, explaining why YAG nanocrystals are not very often encountered in the literature, on the contrary to fluorides. In addition, to use Nd^{3+}-doped nanocrystals in bio-imaging, it is essential to develop nanocrystals with controlled size (targeted size < 100 nm for efficient blood circulation and cell uptake). The latter is especially relevant since the presence of volume

and surface defects strongly damage the fluorescence properties, by favoring non-radiative de-excitations at the expense of the radiative emission.

We recently reported the modified solvothermal synthesis of YAG nanocrystals.[26] By combining high temperature with steady high pressure, we managed to control the nucleation and growth mechanisms of YAG nanocrystals and obtained well-crystallized Ce^{3+}-doped nanocrystals exhibiting internal quantum yields, around 50 %, twice higher than reported in previous work.[26, 27] When doped with Nd^{3+}, such nanocrystals exhibit a temperature-dependent fluorescence with a thermal sensitivity identical to the one of YAG:Nd^{3+} crystals obtained by combustion.[28,29] Moreover, the crucial advantage of the solvothermal route is the formation of stable colloidal suspensions of YAG:Nd^{3+} nanocrystals in ethanol, on the contrary to most of the other reported syntheses that lead to severe nanocrystal agglomeration induced by thermal treatments. [28,29] The challenge was still to transfer these nanocrystals into aqueous solutions for potential biological applications. Several strategies were reported in the literature, in the case of YAG nanocrystals, such as polyethylene glycol (PEG)-grafting,[30] silanization,[31] use of a co-solvent during the synthesis to modify the nature of surface groups [32] or mesoporous silica coating.[33] However, none of these papers report *in vivo* bio-imaging and only the latter reports *in vivo* toxicity evaluation.

Meanwhile, a very efficient route has been developed to directly prepare highly stable aqueous suspensions of inorganic nanoparticles under soft conditions: it relies on the co-precipitation of metal precursors in the presence of double-hydrophilic block copolymers (DHBC) constituted of a metal-complexing block, typically poly(acrylic acid) (PAA) and a highly water soluble block such as polyacrylamide (PAM) or PEG. Those polymers have shown to be very efficient in the growth control and the stabilization of inorganic nanoparticles including metal (Al, La, Cu)

hydroxides,[34,35] and double-hydroxides (Mg-Al, Cu-Al Layered Double Hydroxides), [36,37] oxides (CuO), phosphates ($AlPO_4$) and sulfides (ZnS).[38] In these cases, the nanoparticle size can be controlled directly in aqueous solution at temperatures below 100 °C. The colloidal stability of the obtained nanoparticles was shown to be outstanding, even in the presence of a high amount of salt [34] and their biocompatibility also proved to be excellent.[39,40] However, DHBC have not yet been used to stabilize nanoparticles that were previously prepared under more severe conditions, i.e. high temperature and high pressure, which is the case of YAG nanocrystals.

Here, we report the solvothermal synthesis and morphological characterizations of Nd^{3+}-doped YAG nanocrystals and, more specifically, their stabilization in aqueous solution by poly(acrylic acid)-b-polyacrylamide (PAA-b-PAM) copolymers. Subsequently, we assessed the optical properties of these polymer-stabilized YAG:Nd^{3+} nanocrystals, demonstrate their nanothermometry properties, and their strong potential for *in vivo* imaging.

2. Experimental Section

Synthesis of $Y_{2.94}Nd_{0.06}Al_5O_{12}$ nanocrystals. Yttrium acetate tetrahydrate (1.88 mmol), neodymium acetate hydrate (0.04 mmol) and aluminum isopropoxide (3.20 mmol), all purchased from Sigma Aldrich (purity > 99.9 %) were dispersed in 18 mL of 1,4-butanediol (purity of 99%, Alfa Aesar) and stirred for 48 h at room temperature. 0.5 mL of this mixture was transferred into a sapphire tube and placed in-between two pistons that will deliver the pressure onto the solution. The vessel was introduced into a home-made autoclave, described in [41]. The pressure, controlled by He gas and transferred to the solution via the two pistons, was set at 200 bar. Then, the temperature was increased to 400 °C, with a heating ramp of 50 °C/min and maintained constant during 2.5 h of

synthesis. After cooling down, the solution was retrieved and washed by successive centrifugations in ethanol. Finally, the nanocrystals were dispersed in ethanol with a typical concentration of 10 g/L. Note that the Nd^{3+} doping concentration was set at 2 mol.%, based on previous studies on YAG:Nd^{3+} ceramics, demonstrating that Nd^{3+} segregation occurred for concentrations between 1 and 3 mol.%[42,43] and that fluorescence intensity decreases for concentrations larger than 3 mol.%.[43] However, as the incorporation rate and spatial distribution of the doping ions depends on the synthesis process, it would be interesting in future work to optimize the Nd^{3+} concentration in the nanocrystals produced by this reported solvothermal method.

Functionalization by poly(acrylic acid)-b-polyacrylamide DHBC. The used poly(acrylic acid)-*b*-poly(acrylamide) (PAA-*b*-PAM) DHBC is composed of a PAA metal-binding block which is smaller than the PAM neutral block. The number-averaged molecular weights (M_n) of the PAA and PAM blocks are 2000 and 20 000 g/mol, respectively, and are indicated close to each block name: PAA_{2k}-*b*-PAM_{20k}. In the text, for sake of conciseness, the copolymer is named: PAA-b-PAM. It was prepared according to a well-established sequential polymerization of acrylic acid and acrylamide (Sigma Aldrich) performed in a hydroalcoholic medium in the presence of a xanthate RAFT/MADIX transfer agent (Rhodia).[44] A PAA-b-PAM solution was prepared by dissolving 40 mg of copolymer in deionized water (c = 5 g/L). 10 mL of the copolymer was added to 10 mL of the nanocrystal alcoholic solution (c = 1 g/L) and the mixture was sonicated in an ultrasonic bath for 4 h at 45 °C. After centrifugation, the obtained nanocrystals were dispersed in deionized water (pH = 7) or PBS, with a typical concentration of 1 mg/mL.

Structural characterization. Transmission electron microscopy (TEM) images of YAG:Nd^{3+} nanocrystals were recorded using a Philips CM300 microscope, operating at 300 kV and equipped with a TemCam F416 TVIPS camera. The sample preparation consisted of evaporating droplets

of nanocrystals strongly dispersed in ethanol onto carbon grids. Fourier-transform infrared (FTIR) spectroscopy was performed using a Nicolet iN10 spectrometer on dried powder samples, mixed with KBr powder in a 1:75 weight ratio and shaped into pellets. The measurements were performed under vacuum to avoid parasite peaks from air, especially N_2 gas.

Optical measurements. Fluorescence of water dispersed YAG:Nd^{3+} nanocrystals (1 mg/mL) excited under 793 nm laser excitation was recorded using NIR detector (Shamrock 500i monochromator, iDus InGaAs 1.7 NIR camera). A 830LP filter (Semrock Inc.) was used to remove scattered excitation light. The temperature induced change of fluorescence was recorded within the 20-45 °C range, considering that traditional hyperthermia treatments increases the temperature in the area of interest to 41-48 °C to kill the cancer cells and to protect surrounding healthy tissue. The fluorescence intensity ratio (FIR) for each temperature value was estimated from the ratio of the integrated fluorescence intensities (I_1 and I_2) of the two temperature sensitive Nd^{3+} emission bands at around 950 nm (corresponding to the $^4F_{3/2} \rightarrow {}^4I_{9/2}$ transition). Fluorescence decays were recorded using an Optical Parametric Oscillator (OPO Lotis TII LT-2214) pumped by the third harmonic of a 10 ns Nd:YAG Q-Switched laser. The OPO provides 10 ns pulses of 808 nm wavelength. Pulse energy and repetition rates were 4mJ and 10 Hz, respectively. The 808 nm wavelength beam was focused into the colloidal suspension of YAG:Nd^{3+} nanocrystals by using a simple 10 cm focal lens. The emitted radiation was collected by an optical system and coupled to a compact monochromator (Kymera 193i from Andor) tuned to 1060 nm passing radiation at this wavelength on to an infrared photomultiplier (Hamamatsu Photonics). The decay curve was registered and averaged with a digital oscilloscope (LeCroy Waverunner 6050A).

In vivo experiments.

Animal studies: 1 CD1 3-month-old mouse was employed in this study. All animal experiments were approved by the Animal Ethics Committee of the Universidad Autónoma de Madrid and conducted in accordance with the European Union directive 63/2010UE and the Spanish regulation RD 53/2013. The injection of 150 µl of a dispersion (1 mg/mL) of YAG:Nd^{3+}-(PAA-b-PAM) nanocrystals in PBS directly into the stomach of the animals was performed with a bulb-tipped gastric gavage needle by mouth. Anesthesia was performed via isoflurane inhalation (4-5% induction, 2% maintenance). After the experiment, the mouse was euthanized and the freshly dissected organs analyzed.

Hyperspectral imaging (HSI): An 808 nm fiber-coupled diode laser (LIMO) was employed to excite freshly excised organs through the 808 nm fiber placed next to the camera objective lens with the power and distance adjusted to achieve an illumination intensity of 50 mW/cm^2. All hyperspectral imaging studies selected 20 s exposure time and 10 nm spectral resolution. A short-pass filter (Thorlabs FES0850) was placed directly in front of the laser fiber to minimize specular and diffuse reflection effects. The scattered light from the sample was passed through two continuous long-pass filters (Thorlabs FL0850) to suppress the signal from the laser. Using tubular and short-wave infrared (SWIR) lenses as relays, a fluorescence image is created on the Bragg tunable filter (BTF), allowing the selection of specific wavelengths of incident light. After the second tube lens is focused, the filtered infrared camera (ZephIRTM 1.7) produces a monochromatic image, and the non-filtered light follows a different optical path. In order to cover a specific spectral range, each monochrome image needs to be acquired and stored in the computer, while setting the angle of the BTF rotating stage to the next wavelength. Angle tuning allowed to build the HSI cube, which is a three-dimensional spatial map of spectral changes: the first two dimensions provide spatial information, and the third dimension is responsible for spectral

information. The intensity values of specific pixels in its cube characterize its unique spectral fingerprint.

3. Results

3.1. Stabilization of YAG:Nd^{3+} by the PAA-b-PAM copolymer

YAG:Nd^{3+} nanocrystals (2 mol%, $Y_{2.94}Nd_{0.06}Al_5O_{12}$) were synthesized by a modified-solvothermal process, involving the application of steady high pressure (200 bar) and high temperature (400 °C). The synthesis procedure, reported in the *Experimental Section*, was adapted from [26]. The nanocrystal morphology was studied by transmission electron microscopy (TEM) and shown in **Figure 1**. In addition, a size histogram was plotted by analyzing over 120 nanocrystals in the TEM images (**Figure 1d**) leading to an average nanocrystal size of 85 ± 25 nm. High-magnification TEM images demonstrated high crystallinity as atomic planes running across the whole nanocrystals, up to the edges, are visible (**Figures 1b and 1c**). Fourier transform analysis (inset of **Figure 1b**) and homogeneous contrast on the TEM images also confirm the high crystal quality. The atomic planes observed, (220) and (420), (**Figure 1c**), confirm the garnet-type crystal structure of the synthesized nanocrystals, in agreement with the X-ray diffraction (XRD) pattern (**Figure S1, ESI**). It is essentially the use of high temperature (400 °C) coupled with a pressure of up to 200 bar during solvothermal synthesis that has made possible to obtain individual nanocrystals of high crystalline quality, as earlier tests carried out at lower synthesis temperatures and lower pressure led to poor crystallinity (**Figure S2, ESI**).[26]

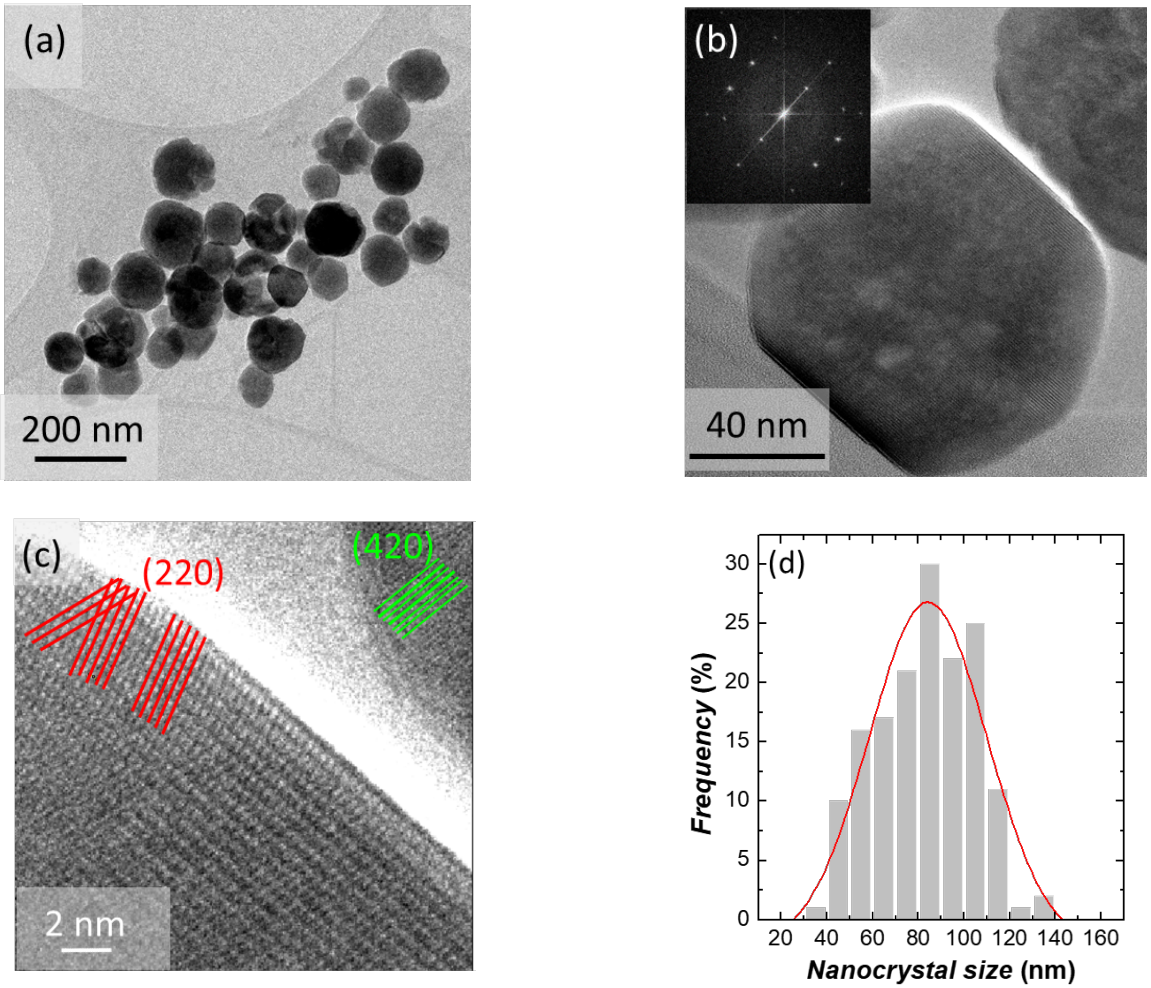

Figure 1. *(a), (b), (c) TEM images of YAG:Nd^{3+} nanocrystals at different magnifications. In the inset of (b) is shown a Fourier transform of the nanocrystal. (c) Atomic planes (220) and (420) of the nanocrystal. (d) Nanocrystal size histogram obtained from the analysis of TEM images.*

After synthesis, successive washings and centrifugations, the pristine YAG:Nd^{3+} nanocrystals were easily dispersed in ethanol owing to their capping layer of butanediol molecules, **Figure 2a, left**.[45] However, YAG nanocrystals are not colloidally stable in aqueous solutions with their butanediol molecular corona. Therefore, to ensure their colloidal stability after transfer from ethanol to water, a stabilization by double hydrophilic block copolymers (DHBC) was performed.

Poly(acrylic acid)-b-polyacrylamide DHBC, with block molecular weights of respectively n = 2000 and m = 20 000 (PAA_{2k}-b-PAM_{20k}), further labelled PAA-b-PAM, were chosen for their capacity to complex metal ions and their high solubility in water. The role of the PAA block is to anchor on the inorganic nanocrystal, while the longer PAM chain provides colloidal stability in water thanks to steric effect.[46,47]

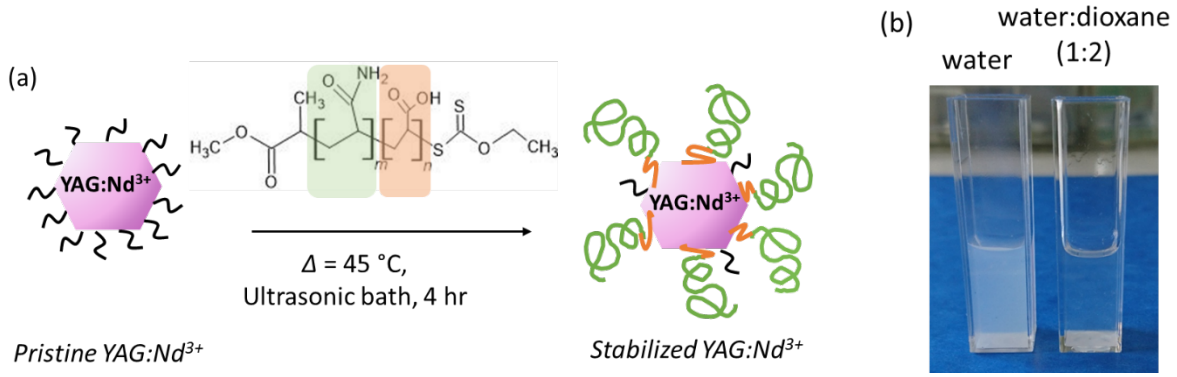

Figure 2. *(a) Scheme of the stabilization of pristine YAG:Nd^{3+} nanocrystals with PAA-b-PAM copolymer. (b) Photographs of colloidal suspensions of stabilized YAG:Nd^{3+} nanocrystals in water (left) and a loss of colloidal stability of stabilized YAG:Nd^{3+} nanocrystals in a mixture of water and dioxane (1:2, v/v) inducing a strong nanocrystal precipitation at the bottom of the cuvette (right).*

The stabilization was performed by dispersing pristine YAG:Nd^{3+} nanocrystals and PAA-b-PAM in a water and ethanol solution (1:1, v/v), in an ultra-sonic bath for 4 hours at 45 °C as illustrated in **Figure 2a**. More details regarding the nanocrystal and copolymer concentration are given in the *Experimental Section*. The solution was then centrifuged to remove the supernatant and the obtained nanocrystals were then easily redispersed in pure water (pH = 7).

The presence of copolymers anchored at the nanocrystal surface is further assessed by different techniques, the first one being the addition of dioxane. **Figure 2b, left,** shows a photograph of a cuvette containing YAG:Nd^{3+} nanocrystals well-dispersed in water after the copolymer treatment (c = 0.5 mg/mL). In stark contrast, in a water and dioxane mixture solution (1:2, v/v), the nanocrystals precipitate (c = 0.5 mg/mL, **Figure 2b, right**) and the supernatant becomes clear, as dioxane is known to be a bad solvent for the polyacrylamide block.[48] Thus, this direct observation indicates that the polyacrylamide chains are present at the surface of the nanocrystals and shrink in the presence of dioxane leading to a loss of steric nanocrystal stabilization and therefore, to a loss of colloidal stability.

Fourier-transform infrared (FTIR) characterization was also performed on the as-grown pristine YAG:Nd^{3+} nanocrystals (further labelled YAG:Nd^{3+}), on the copolymer-stabilized YAG:Nd^{3+} nanocrystals (YAG:Nd^{3+}-(PAA-b-PAM)), and on the PAA-b-PAM copolymer itself (**Figure 3a**). The FTIR spectrum of the YAG:Nd^{3+} nanocrystals (**Figure 3a, pink curve**) exhibit typical low frequency peaks, resulting from the YAG structure, with the peaks at 440 and 565 cm^{-1} corresponding to AlO_6 octahedra, the peaks at 690 and 790 cm^{-1} to AlO_4 tetrahedra and the peak at 725 cm^{-1} to Y-O bonding.[30,49] In addition, the peak at 1060 cm^{-1}, corresponding to the stretching mode of C-O, indicates the presence of alcohol groups at the surface of the YAG nanocrystals, in agreement with the capping layer of 1,4-butanediol, which is the solvent involved in the solvothermal process.[45] In the spectrum of YAG:Nd^{3+}-(PAA-b-PAM) nanocrystals (**Figure 3 a, blue curve and Table S1)**, in addition to the peaks attributed to YAG, peaks corresponding to organic groups are visible, such as 1460 cm^{-1} ($-CH_2$), 1570 cm^{-1} (COO), 1675 cm^{-1} (amide), 2930 cm^{-1} ($-CH_2$) and 3190 cm^{-1} peaks (amide) (black lines on **Figure 3a**),[50,51] confirming the presence of the copolymer. Moreover, in comparison with the spectrum of the YAG:Nd^{3+} nanocrystals, one

can notice the presence of peaks attributed to primary alcohol (1060 cm^{-1} and 3630 cm^{-1}), attesting the presence of remaining butanediol chains.

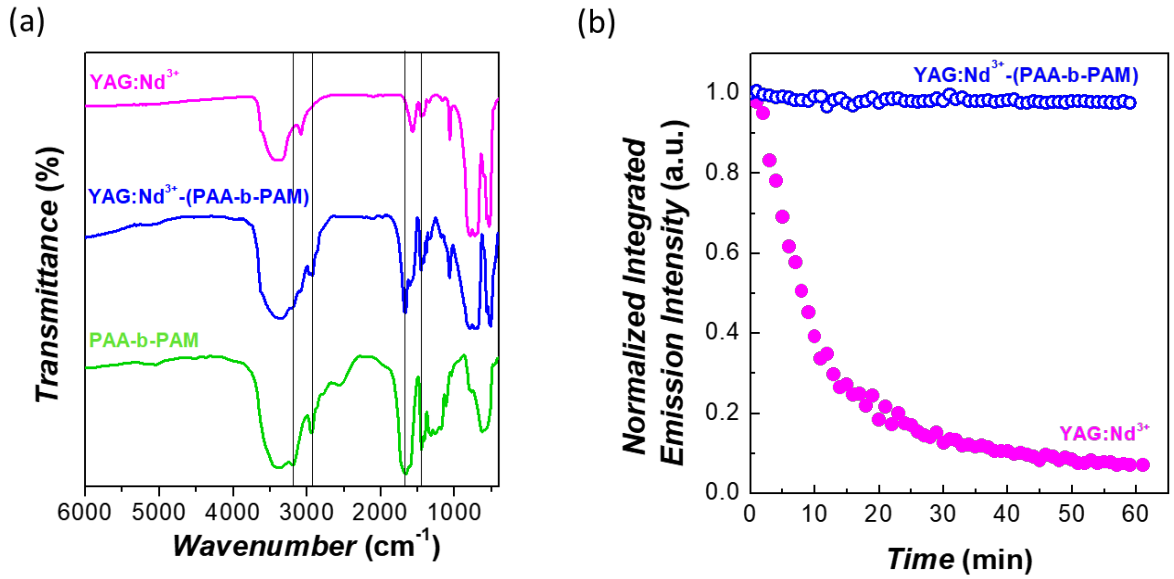

Figure 3. *(a) FTIR characterization of the pristine YAG:Nd^{3+} nanocrystals, of YAG:Nd^{3+} nanocrystals stabilized with the PAA-b-PAM block copolymer and of the pure copolymer. The main peak differences are highlighted by the black lines. (b) Temporal evolution of normalized integrated emission intensity (1061-1075 nm) of pristine YAG:Nd^{3+} and stabilized YAG:Nd^{3+}-(PAA-b-PAM) nanocrystals in water.*

Finally, the YAG:Nd^{3+} and YAG:Nd^{3+}-(PAA-b-PAM) nanocrystals were dispersed in water and the fluorescence intensity of these solutions at 1060 nm was measured over time, under a 793 nm excitation in the upper part of solutions (**Figure 3b**). The integrated fluorescence intensity (1061-1075 nm) of the YAG:Nd^{3+}-(PAA-b-PAM) nanocrystals remain perfectly stable for one hour, while that of the YAG:Nd^{3+} nanocrystals quickly decreases due to their sedimentation, with a

reduction of 60 % over 10 min. It proves that the copolymers are indeed anchored at the surface of the nanocrystals, giving them a very good colloidal stability in water.

3.2. Optical properties of stabilized YAG:Nd^{3+} nanocrystals

The fluorescence of both YAG:Nd^{3+} and YAG:Nd^{3+}-(PAA-b-PAM) nanocrystal aqueous colloidal solutions were recorded over a wide spectral range (850-1500 nm) under 793 nm excitation and indicated no difference in terms of spectral shape. The fluorescence spectra are typical of that of Nd^{3+}, with emission bands around 900 nm, 1.1 µm and 1.3 µm, corresponding to the $^4F_{3/2} \rightarrow {}^4I_{9/2}$, $^4F_{3/2} \rightarrow {}^4I_{11/2}$ and $^4F_{3/2} \rightarrow {}^4I_{13/2}$ electronic transitions, respectively (**Figure 4a**).

The most intense emission peak is observed at 1066 nm, with a full width at half maximum (FHWM) of 5 nm, obtained by a Gaussian fit. This value is larger than the one measured on YAG:Nd^{3+} nanopowder, obtained through heat-treatment (combustion, annealing, etc) (~ 2 nm).[25,52] However, the observation of a sub-structure is a good indicator of the high crystal quality of these nanocrystals as already characterized by XRD and TEM. For reference, in Nd^{3+}-doped glasses, where Nd^{3+} is an amorphous environment, leading to a large inhomogeneous broadening, the FWHM is of the order of ~ 25 nm.[53] The narrow emission line at 1066 nm, combined with good colloidal properties in water, is thus favorable for *in vivo* detection in the second biological window.

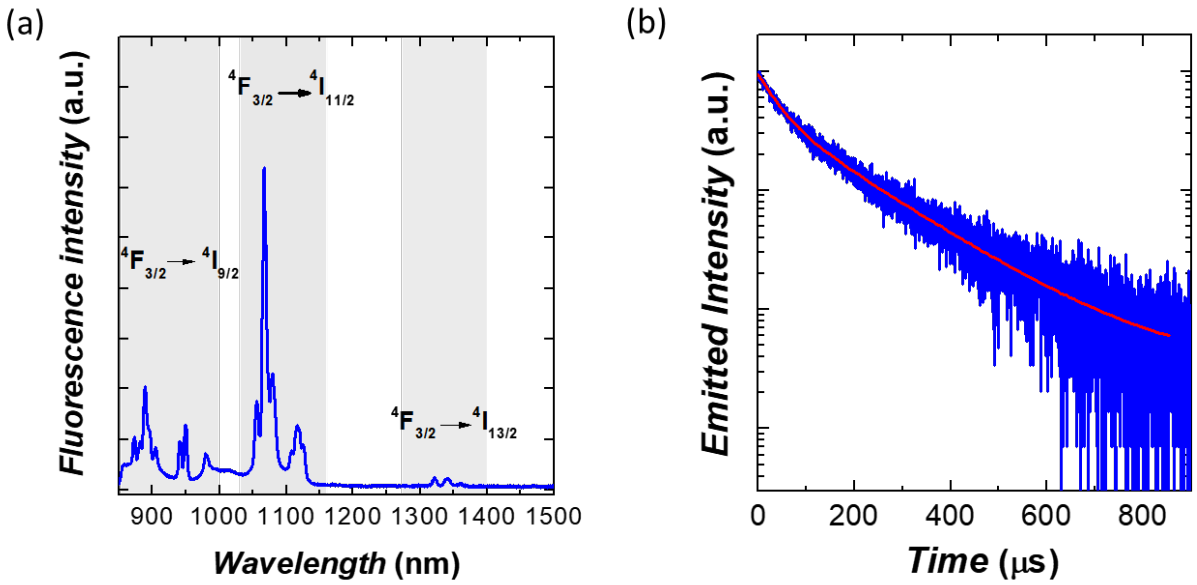

Figure 4. *(a) Fluorescence spectrum of stabilized YAG:Nd^{3+}-(PAA-b-PAM) nanocrystals in aqueous solution. (b) Fluorescence decay at 1060 nm of YAG:Nd^{3+}-(PAA-b-PAM) nanocrystals in PBS solution, with the bi-exponential fit, leading to two characteristics decays: τ_1 = 42 μs and τ_2 = 168 μs.*

The fluorescence lifetime of the $^4F_{3/2}$ metastable excited state of Nd^{3+} in YAG:Nd^{3+}-(PAA-b-PAM) nanocrystals measured under 808 nm pulsed excitation (**Figure 4b**) revealed a bi-exponential decay, leading to two characteristic decay times: τ_1 = 42 μs and τ_2 = 168 μs, in equivalent proportions (average lifetime, τ ~ 105 μs – details regarding its calculation are given in SI). The bi-exponential decay indicates the presence of two types of Nd^{3+} ions in YAG:Nd^{3+}-(PAA-b-PAM) nanocrystals: one, characterized by a short τ_1, most likely corresponds to Nd^{3+} ions at the surface of the nanocrystals, whereas the other, characterized by a much longer τ_2, corresponds to Nd^{3+} ions in the core of the nanocrystals. In comparison, the lifetime of this state in bulk YAG:Nd^{3+} single crystals or ceramics is longer (~ 250 μs).[54] The shortening of the lifetime in nanocrystals in aqueous solution is generally observed and is explained by the presence of the solvent (water) and

of the molecules at their surface. [55,56] In the present case, both water and copolymers, in particular the PAA block anchored to the nanocrystal, in close vicinity to the Nd^{3+} situated at the surface, are responsible for non-radiative de-excitations due to their large phonon energy (~ 3000 cm^{-1} as assessed by FTIR, **Figure 3a**). Taking this phenomenon into account, the average lifetime measured in these stabilized YAG:Nd^{3+} nanocrystals is relatively long, with respect to the values found in other Nd^{3+}-doped YAG nanocrystals. For example, the reported lifetime of the $^4F_{3/2}$ state in YAG:Nd^{3+} nanocrystals synthesized by conventional co-precipitation is 75 µs.[57] Despite the presence of organic groups at the surface of the nanocrystals (**Table S1**), the good crystal quality of the nanocrystals minimizes the non-radiative de-excitations due to crystal defects and ensures a relatively long lifetime.

Hence, the optical properties of the YAG:Nd^{3+}-(PAA-b-PAM) nanocrystals are very promising for *in vivo* bio-imaging, which is investigated hereafter. Beforehand, these nanocrystals were transferred to a cell-compatible medium, such as a phosphate-buffered saline (PBS) solution. To ensure the colloidal stability in this environment, dynamic light scattering (DLS) measurements were performed on the YAG:Nd^{3+}-(PAA-b-PAM) nanocrystals dispersed in water at 25 °C and in PBS at 37 °C (**Figure 5**). Under these different conditions the nanocrystal size remains similar, around 120 nm, while the colloidal stability is perfectly preserved. The slight difference between the diameter values obtained in water at 25 °C and in PBS at 37 °C could be explained by the interactions between the copolymer and the different ions present in PBS.

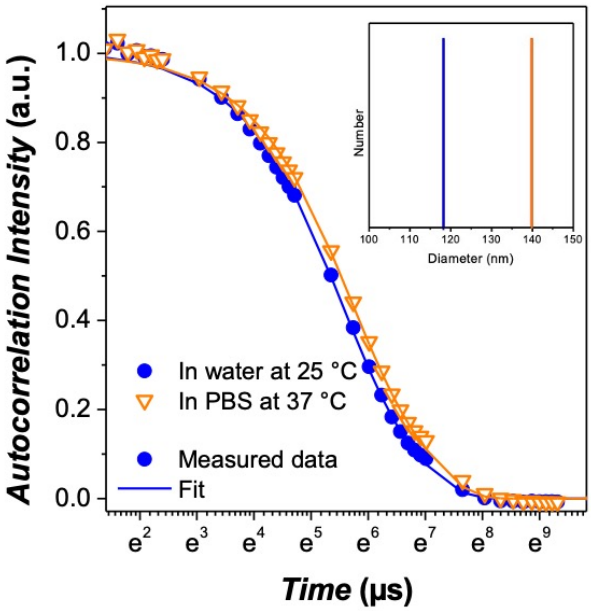

Figure 5. *Normalized intensity autocorrelation functions (IACF) of the YAG:Nd^{3+}-(PAA-b-PAM) nanocrystal colloidal solutions in water at 25 °C and in PBS at 37 °C. A fitting of the IACF, performed following the well-known method of cumulants,[58] allows access the values of the mean time-decay τ_c, which is associated to the hydrodynamic diameter of the nanocrystals and that of the polydispersity index (PDI), related to the width of the diameter distribution. Inset: graph showing the diameter of the YAG:Nd^{3+}-(PAA-b-PAM) nanocrystals in water at 25 °C and in PBS at 37 °C.*

3.3. Bio-imaging

In order to demonstrate the potential of YAG:Nd^{3+} nanocrystals as fluorescent probes for *in vivo* imaging, 150 µl of a solution of YAG:Nd^{3+}-(PAA-b-PAM) nanocrystals in PBS (1 mg/mL) were orally administrated to a CD1 mouse. After administration the mouse was anesthetized and placed in a NIR-II hyperspectral imaging setup. Optical excitation was performed with an 808 nm fiber coupled laser diode. The spot size at the animal´s location was 10 cm^2 and the on-target laser power

was varied between 1 and 5 W. In these experiments, 800 nm wavelength radiation was selected as it leads to a minimum excitation of autofluorescence and, simultaneously, to a minimum thermal loading caused by parasitic tissue absorption.[59,60] **Figure 6** summarizes the results obtained from the hyperspectral imaging experiments. The hyperspectral imaging set-up enables the acquisition of the fluorescence images of the mice at different wavelengths ranging from 900 to 1700 nm. The analysis of the hyperspectral cube thereby allows the acquisition of pixel-by-pixel fluorescence spectra. **Figure 6a** includes the autofluorescence spectra as obtained from a control CD1 mouse. It is evidenced that the endogenous pigments of both skin and internal organs lead to a broad autofluorescence tail ranging from 900 to 1200 nm. The autofluorescence spectrum also accounts for a sharp peak at around $\lambda_1 \approx 1050$ nm that has been recently attributed to the endogenous autofluorescence of lipids.[61] For the sake of comparison, **Figure 6a** also includes the fluorescence spectrum as obtained in the same hyperspectral imager from a solution containing only the YAG:Nd^{3+}-(PAA-b-PAM) nanocrystals. The three bands originating from the $^4F_{3/2}$ metastable state are observed with the maximum fluorescence intensity generated at $\lambda_2 \approx 1070$ nm corresponding to the peak emission from the $^4F_{3/2} \rightarrow {}^4I_{11/2}$ transition. The difference to the above measured 1066 nm emission stems from the spectral resolution of the hyperspectral system which is 5 nm (so the emission line of YAG:Nd^{3+}-(PAA-b-PAM) nanocrystals from the $^4F_{3/2} \rightarrow {}^4I_{11/2}$ is detected by our hyperspectral system at 1070 nm). From **Figure 6a**, it is evident that a large overlap between autofluorescence and YAG:Nd^{3+}-(PAA-b-PAM) fluorescence does exist but the fact that they present two sharp peaks opens the possibility of selective imaging of YAG:Nd^{3+}-(PAA-b-PAM) nanocrystals by differential imaging. **Figure 6b** shows the fluorescence image as obtained for a fluorescence emission wavelength $\lambda_1 \approx 1050$ nm of the mouse after oral administration of YAG:Nd^{3+}-(PAA-b-PAM) nanocrystals. A clear fluorescence signal originates from the abdomen

and is mainly attributed to the autofluorescence generated by the liver and digestive apparatus. **Figure 6c** shows a fluorescence image of the same mouse as in **Figure 6b** but obtained for an emission wavelength of $\lambda_2 \approx 1070$ nm. At first glance, both images are virtually identical although some additional signal on the left flank of the animal is detected that can be attributed to the presence of YAG:Nd^{3+}-(PAA-b-PAM) nanocrystals. Differential imaging consists in the subtraction of two fluorescence images obtained at two different but close wavelengths. In particular, the fluorescence signal stemming only from YAG:Nd^{3+}-(PAA-b-PAM) nanocrystals can be isolated by subtracting the fluorescence image at $\lambda_1 \approx 1050$ nm (autofluorescence background) from the fluorescence image obtained for $\lambda_2 \approx 1070$ nm. The resulting fluorescence image is shown in **Figure 6d**. The autofluorescence background has been substantially removed and it is clear now that the fluorescence signal is only detected at the stomach and upper area of intestine. This was, indeed, expected as the YAG:Nd^{3+}-(PAA-b-PAM) nanocrystals were administrated orally, but this result is a perfect illustration of the potential of these nanocrystals to mostly remove the parasitic background thanks to their narrow emission lines.

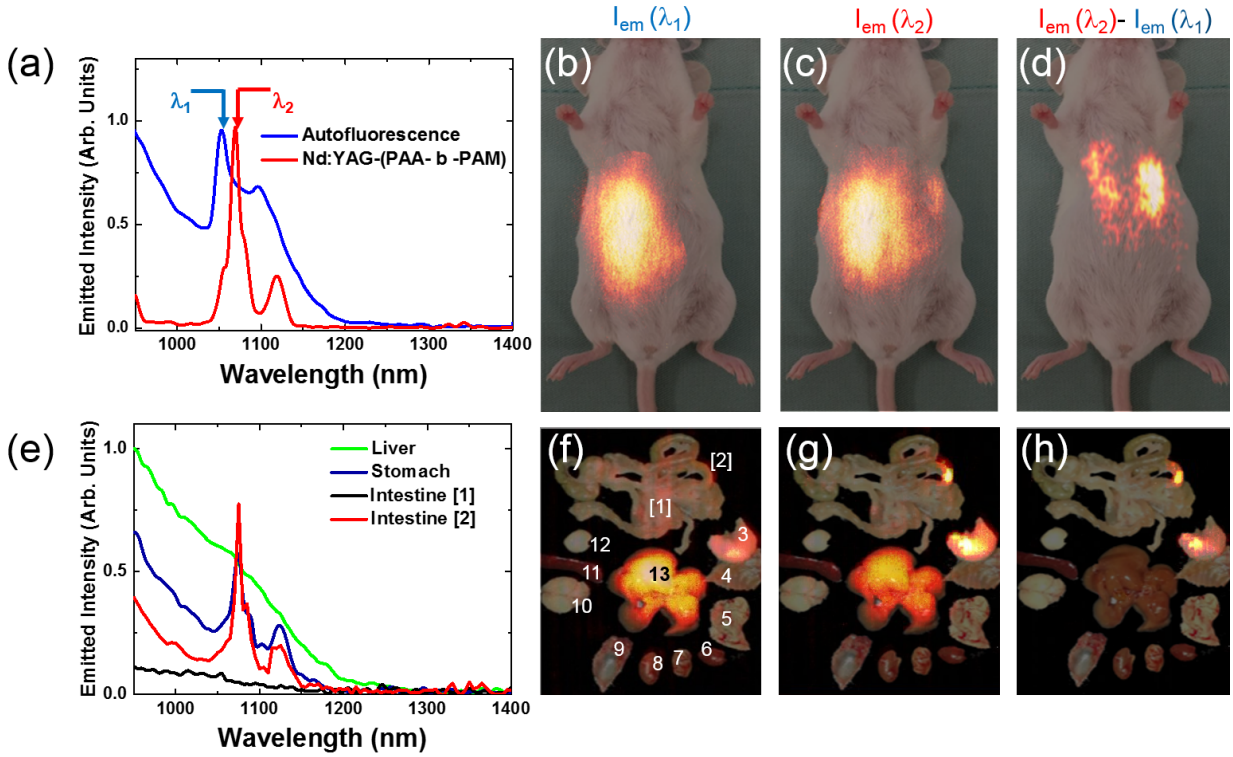

Figure 6. *Differential hyperspectral fluorescence in vivo imaging with stabilized YAG:Nd^{3+} -(PAA-b-PAM) nanocrystals. (a) Emission spectra of the whole body autofluorescence as obtained from a control CD1 mouse. Emission spectrum generated by a colloidal solution of YAG:Nd^{3+}-(PAA-b-PAM) nanocrystals in PBS. The two emission wavelengths used in this work for differential fluorescence imaging are indicated as λ_1 (autofluorescence) and λ_2 (emission of YAG:Nd^{3+}-(PAA-b-PAM) nanocrystals).* ***(b)*** *In vivo fluorescence image of a CD1 mouse after oral administration of YAG:Nd^{3+}-(PAA-b-PAM) nanocrystals as obtained for an emission wavelength of $\lambda_1 \approx 1050$ nm.* ***(c)*** *In vivo fluorescence image of a CD1 mouse after oral administration of YAG:Nd^{3+}-(PAA-b-PAM) nanocrystals as obtained for an emission wavelength of $\lambda_2 \approx 1070$ nm.* ***(d)*** *In vivo differential (λ_2-λ_1) fluorescence image of the mouse after oral administration of YAG:Nd^{3+}-(PAA-b-PAM) nanocrystals.* ***(e)*** *Ex vivo fluorescence spectra generated from different organs extracted from a CD1 mouse after oral administration of YAG:Nd^{3+}-(PAA-b-PAM)*

nanocrystals. ***(f)*** *Ex vivo fluorescence images of different organs extracted of a CD1 mouse after oral administration of YAG:Nd^{3+}-(PAA-b-PAM) nanocrystals as obtained for an emission wavelength of $\lambda_1 \approx 1050$ nm.* ***(g)*** *Ex vivo fluorescence images of different organs extracted of the mouse after oral administration of YAG:Nd^{3+} nanocrystals as obtained for an emission wavelength of $\lambda_2 \approx 1070$ nm.* ***(h)*** *In vivo differential (λ_2-λ_1) fluorescence image of the organs extracted from the mouse after oral administration of YAG:Nd^{3+} nanocrystals. In (f), (g) and (h), the numbers from 1 to 13 denote 1: intestine [1], 2: intestine [2], 3: stomach, 4: ribs + intercostal muscles, 5: lungs, 6: heart, 7: pancreas, 8: kidney, 9 skull, 10 brain, 11: spleen, 12: thymus, and 13: liver.*

After these *in vivo* images and to go further in this proof of concept, the animal was sacrificed and the organs were analyzed. **Figure 6e** shows the PL spectra obtained for the liver, stomach and the entrance of the intestine and the center of the organ. Note that in all cases, the autofluorescence tail is dominant. The presence of the emission peak at 1070 nm, indicator of the presence of YAG:Nd^{3+}-(PAA-b-PAM) nanocrystals, is only observed in the stomach and, in some extent, in the intestine. In order to further confirm the presence of YAG:Nd^{3+}-(PAA-b-PAM) nanocrystals in the stomach and intestine, differential fluorescence imaging was also applied to the *ex vivo* fluorescence images of all the organs. **Figures 6f** and **6g** include the fluorescence images of all the organs as obtained at 1050 and 1070 nm emission wavelength, respectively. **Figure 6h** shows the differential fluorescence of all the organs where the presence of YAG:Nd^{3+}-(PAA-b-PAM) nanocrystals is only observed in the stomach and first sections of the intestine as expected upon oral administration.

3.4. Nanothermometry

In addition to the need for nanoprobes for bio-imaging, NIR fluorescence contrast agents with integrated optical temperature sensing are in high demand for various biomedical applications. Solely Nd^{3+} doped luminescent nanothermometers have shown proficiency for temperature readout through any of the three main Nd^{3+} NIR transitions.[18,21,62,63,64]. To date, the most intensively studied single band Nd^{3+} nanothermometers typically employ the $^4F_{3/2} \rightarrow {}^4I_{9/2}$ emission and the fluorescence intensity ratio (*FIR*) is determined from the intensities of the selected R_1, R_2 - $Z_{i,j}$ (where i and j can be equal) transitions between the sublevels of the split electronic states.[28,29,65] The emission peaks corresponding to the R_1, $R_2 \rightarrow Z_5$ transitions (**Figure 7a**) are better spectrally separated than others, making them more compliant for ratiometric temperature evaluation.

Here, ratiometric fluorescence nanothermometry measurements of YAG:Nd^{3+}-(PAA-b-PAM) nanocrystals were implemented through two emission peaks at around 941 and 949 nm, which correspond to emission from the thermally coupled R_1 and R_2 Stark sublevels of the $^4F_{3/2}$ state to the $^4I_{9/2}$ state. The normalized emission spectra showed a relative decrease in the intensity of the lower energy transition ($R_1 \rightarrow Z_5$) in the YAG:Nd^{3+}-(PAA-b-PAM) nanocrystals (**Figure 7b**), associated to a change in the population of the R_1 and R_2 sublevels as the temperature increases, which is ruled by the Boltzmann distribution.[66] The FIR of the two emission peaks of the YAG:Nd^{3+}-(PAA-b-PAM) nanocrystals was calculated as a ratio of integrated intensities I_2 (938.7-943.7 nm) and I_1 (947.1-952.1 nm). FIR increased with increasing ambient temperature in the 20–45 °C range (**Figure 7c**) leading to the relative thermal sensitivity (S_r) of 0.20 % °C^{-1} at 20 °C, calculated as $S_r = 1/LIR * \delta LIR/\delta T$ (**Figure 7e**). Very similar S_r values (0.19 % °C $^{-1}$ at 20 °C) were calculated for pristine YAG:Nd^{3+} nanocrystals showing that the copolymer coating does not affect

thermal sensitivity of the nanocrystals. The *FIR* of stabilized YAG:Nd^{3+}-(PAA-b-PAM) nanocrystals recorded in 9 heating-cooling temperature cycles show the repeatability of around 99.7 % (**Figure 7d**). Further calculations revealed that temperature uncertainty δT of YAG:Nd^{3+}-(PAA-b-PAM) nanocrystals is ~2.1 °C at 20 °C and ~2.3°C at 35 °C, which is comparable with data published on Nd^{3+} doped single-band nanothermometers with different host materials.[18,21,67] These are promising results demonstrating their capability for temperature sensing and further evaluation in different tissues, at different pH values, and for different excitation power densities will allow to determine whether these nanocrystals could also be employed as reliable *in vivo* nanothermometers.[68]

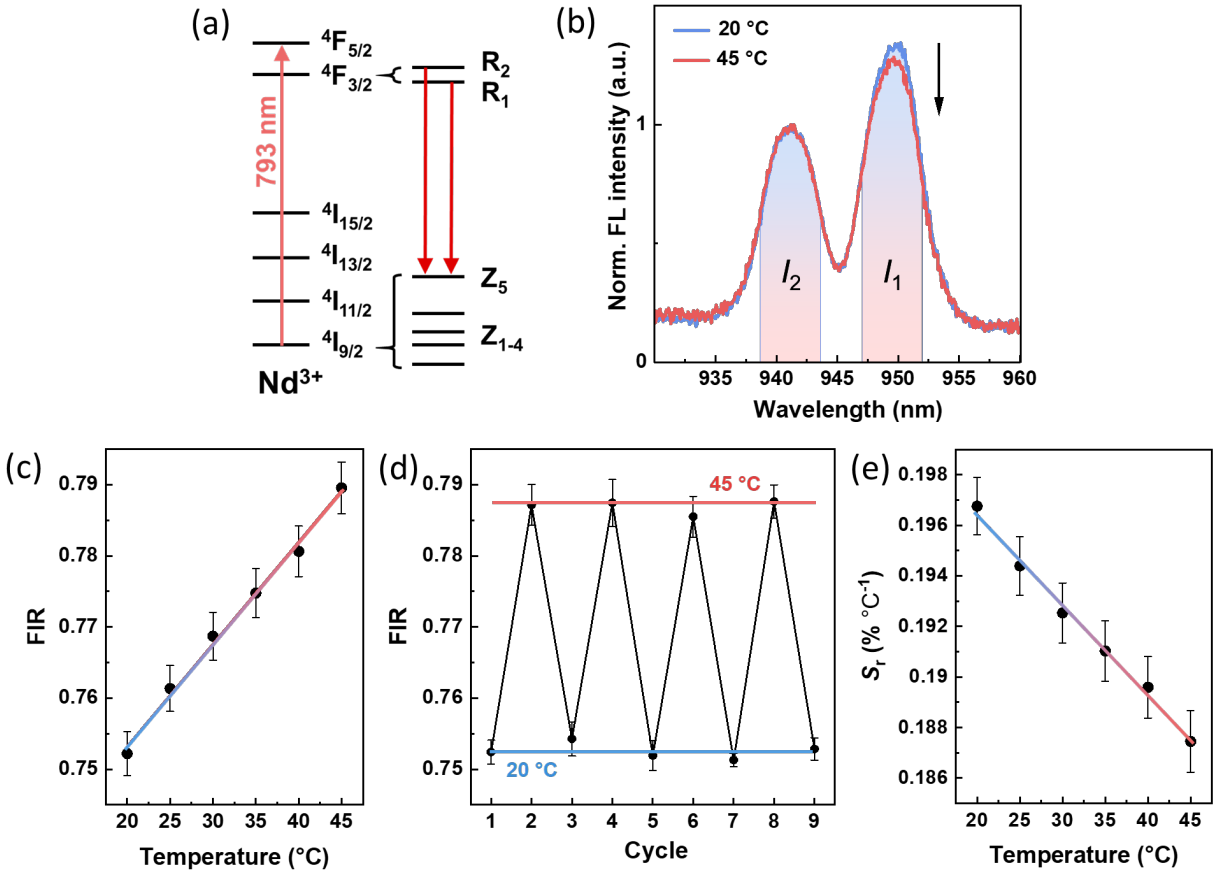

Figure 7. *Nanothermometry of stabilized YAG:Nd^{3+}-(PAA-b-PAM) nanocrystals. (a) Energy level diagram of Nd^{3+}, showing the electronic transitions of interest for the fluorescence nanothermometry measurements. (b) Fluorescence spectra corresponding to R_1, $R_2 \rightarrow Z_5$ transitions of Nd^{3+}, recorded at 20 °C and 45 °C, upon 793 nm excitation. The shaded segments depict integration ranges used for calculations of fluorescence intensity ratios and relative thermal sensitivity. (c) Fluorescence intensity ratio over 20-45 °C temperature range. (d) Repeatability of FIR over 9 cycles between 20 and 45 °C. (e) Relative thermal sensitivity over 20-45 °C temperature range.*

Discussion

Previous works on YAG:Nd^{3+} featured nanocrystals of irregular, inhomogeneous shape and size,[29] making their surface functionalization very difficult. That relevant pitfall greatly hampered proper engineering towards improving their eventual biodistribution, or attaching functional groups to them for a target-based application. Even a higher limitation of such early attempts was the short-lived water dispersibility of such nanocrystals, which limited their scope to *ex vivo* proof-of-concept. For all the aspects above, directly linked to the structural properties of any given nanocrystal, our YAG:Nd^{3+} nanocrystals presented in this work possess much better assets (size below 100 nm and high crystal quality), as corroborated by the data shown in **Figure 1**. The potential for surface modification of the nanocrystals is solidly proven by the successful functionalization (**Figure 2 and Table S1**) through PAA-b-PAM copolymer grafting that we performed on the YAG:Nd^{3+} nanocrystals - a process described in the previous section. This

coating provides them with a high degree of colloidal stability (**Figures 3a and 5**), an asset of paramount importance for a gamut of *in vivo* application of these nanoprobes.

One of the expectable advantages, from the optical point of view, of using an oxide-based luminescent material (namely a garnet) as a host, is narrower emission lines compared with the widely reported fluoride hosts, such as $NaYF_4$, $NaGdF_4$, CaF_2, LaF_3 etc. Meanwhile, the YAG:Nd^{3+} nanocrystals we reported here feature a much sharper spectral profile than those other families of Nd^{3+}-doped nanocrystals. Subsequently, the measured FWHM of the main emission peak centered at ~ 1070 nm (NIR-II) of our YAG:Nd^{3+} nanocrystals is 5 nm, that is a 2-3 fold narrower emission band compared to their fluoride competitors.[25,69] Therefore, YAG:Nd^{3+} nanocrystals have profound implications for applications as nanoprobes for NIR-II bioimaging as well as NIR-I thermal imaging. As described in the previous section, for the *in vivo* imaging we employed a hyperspectral imager that allows us to record signal from a spectral range as reduced as low as 5 nm. This equipment allows for the acquisition of hyperspectral cubes containing whole body fluorescence images obtained in the 900-1700 nm spectral range. The characteristic sharp emission line of YAG:Nd^{3+} nanocrystals at ~1070 nm does not overlap with the main autofluorescence line at 1050 nm attributed to lipids.[61] This allows for efficient filtering, although partial, of the autofluorescence background by applying the differential fluorescence imaging procedure. Although this is not a real-time imaging technique, it still allows for fast *in vivo* imaging, featuring time resolutions in the order of seconds, which, for *in vivo* applications, constitutes a time resolution enough to measure most of thermal processes such as tissue relaxation dynamics.[70] Depending on the selected wavelength range and filters, this can be optimized to imaging times in the range of the integration times necessary for the images (seconds). This direct removal of autofluorescence, demonstrated for the first time in this work, has been proven to be of

high efficiency in decreasing the autofluorescence background and makes it possible to accurately localize *in vivo* YAG:Nd^{3+}-(PAA-b-PAM) nanocrystals in mice after oral administration.

Moreover, the relative thermal sensitivity of 0.20 % °C^{-1} of YAG:Nd^{3+}-(PAA-b-PAM) nanocrystals achieved here is higher than previously reported ones (~0.14 % °C^{-1}) that were also evaluated through R_1, $R_2 \rightarrow Z_5$ transitions of $^4F_{3/2} \rightarrow {}^4I_{9/2}$ single band emission.[28,29] It has been widely reported that nanothermometry parameters such as FIR and S_r are strongly dependent on the physical and chemical properties of the host. Thus, size, shape, and crystalline phase are just a few characteristics of many that can significantly modify the performance of the nanothermometer.[71,72,73,74] Furthermore, in our previous publication on nanothermometry of Nd^{3+}-doped GSAG ($Gd_3Sc_2Al_3O_{12}$) nanocrystals, we have shown that higher temperatures during solvothermal synthesis result in higher crystallinity of garnet nanocrystals of the same composition, and, consequently, higher relative thermal sensitivity.[28] Thus, substantially improved S_r values of YAG:Nd^{3+} nanocrystals reported here suggest higher crystallinity achieved possibly due to higher synthesis temperature (400 °C) used compared to the previously reported protocol (350 °C).

Finally, in a prospective manner oriented towards the future, we must point to the versatility of the copolymer stabilization process used here for the YAG:Nd^{3+} nanocrystals after their solvothermal synthesis. A strategy could be to replace the PAA-b-PAM DHBC by a copolymer whose water-soluble neutral block presents a comb-type architecture, such as a poly(acrylate methoxy poly(ethyleneoxide)) (PAMPEO).[75] For the same molecular weight as the linear neutral chain, a comb-type copolymer is denser and should provide the same stability in water while keeping the overall nanocrystal hydrodynamic diameter smaller. It is also important to note that, in view of the recent reports on standardization of the requirements of luminescent thermometers for *in vivo*

temperature imaging applications,[68] future works we are planning on our YAG:Nd^{3+} nanocrystals will further elaborate on their reliability as nanothermometers, in particular, to provide some additional data such as the quantum yield as measured by absolute methods, and also the necessary evaluation of the self-absorption of the YAG:Nd^{3+} emission lines used for thermal sensing.

Additionally, our YAG:Nd^{3+}-(PAA-b-PAM) nanocrystals as probes for biomedical imaging can and should still be developed further. It must be pointed out that the two emission lines proposed for thermal readout show a large overlap with the infrared autofluorescence of tissues. Moreover, those lines intensity could be sometimes of a similar level as the autofluorescence background, as it is the case of our measurements. In such conditions, *in vivo* thermal reading by means of YAG:Nd^{3+} nanocrystals would be difficult, requiring a more sophisticated approach than just the spectral analysis of fluorescence images. In particular, the autofluorescence background must be removed, and for such purpose additional techniques have to be employed. YAG:Nd^{3+}-(PAA-b-PAM) nanocrystals emission lifetimes are long, i.e. several tens of μs (**Figure 4b)** - orders of magnitude longer than autofluorescence lifetime-, which makes them very attractive candidates for time-gated imaging.[76,77] In fact, the potential use of these YAG:Nd^{3+}-(PAA-b-PAM) nanocrystals for time-gating would put to work their characteristic narrow emission allowing differential imaging together with the drastic removal of residual autofluorescence typical of time-gating, hence the synergy of both techniques converting such nanocrystals into the ultimate autofluorescence-free NIR-II *in vivo* fluorescent sensors, which would also allow to employ them for *in vivo* nanothermometry. Moreover, the well-demonstrated temperature-dependence of Nd^{3+} emission lifetimes, in different crystalline hosts, offers an attractive additional route for developing *in vivo* nanothermometry - additional to the ratiometric approach shown in this work.

Conclusions

This work presents the spectral characteristics of the YAG:Nd^{3+} fluorescent nanomaterial, cleverly synthesized through a novel solvothermal route and functionalized with a biocompatible block copolymer. The emphasis of our findings is not on those spectral assets per se, though. In fact, our imaging results undoubtedly demonstrate how the intrinsically narrow emission lines of YAG:Nd^{3+} nanocrystals are key to bringing forward differential imaging, reported for the first time *in vivo*. Such an innovative approach to autofluorescence removal enables us to get rid of the useless optical background by means of a relatively fast and straightforward subtraction between two images, each of them taken at close spectral range. Though much has been reported about fluoride-based Ln^{3+}-doped nanocrystals, the need for narrower emission lines in order to achieve an almost complete removal of fluorescence indicated the convenience to turn attention towards oxide hosts. Based on the results of this publication, future works dealing with YAG:Nd^{3+} nanocrystals will target the careful tailoring of doping concentration, also trying more diverse surface functionalization of the nanocrystals, in order to expand the portfolio of available applications: i.e. certain specific organs or systems to image in animal models, and tackling molecular imaging as well.

The impact of the results reported are not only restricted to *in vivo* imaging. The nanothermometry performance also discussed here constitutes a real opportunity to factor together such measures as thermal sensitivity in the NIR-I together with the advantages for bioimaging mentioned above. Future steps for these solvothermally synthesized nanocrystals to feasibly increase their potential as preclinical agents should be a two-pronged approach. One way, a further optimization of the brightness of the YAG:Nd^{3+} nanocrystals emission should be carried out, a goal that, for instance, can be implemented by way of YAG:Nd^{3+}/YAG core-shell architecture.[78] On the other hand, it

would be desirable to extend the nanothermometry range of these new YAG:Nd^{3+} nanocrystals beyond 1000 nm, (i.e. NIR-II nanothermometry). That foreseeable synergy between autofluorescence free imaging and temperature sensing, both within NIR-II range, suggests profound future of the YAG:Nd^{3+} multifunctional nanoplatform.

ASSOCIATED CONTENT

Supporting Information.

The following files are available free of charge.

A .pdf file gathering additional structural characterizations of Nd^{3+}-doped nanocrystals.

AUTHOR INFORMATION

Corresponding Author

* geraldine.dantelle@neel.cnrs.fr

Author Contributions

The manuscript was written through contributions of all authors. All authors have given approval to the final version of the manuscript.

ACKNOWLEDGMENT

A.B. acknowledges funding from Comunidad de Madrid through TALENTO grant ref. 2019-T1/IND-14014. F.V. acknowledges funding from the Natural Sciences and Engineering Research

Council (NSERC) of Canada through the Strategic Project Grants, Discovery Grants program and the Discovery Accelerator Supplement (DAS) award, the Canada Foundation for Innovation for infrastructure and its operation, and the Fonds de recherche du Québec – Nature et technologies (FRQNT). C.G. acknowledges M. Destarac (UMR 5623 CNRS-UPS Toulouse, Paul Sabatier Toulouse University) for providing the PAA-b-PAM double-hydrophilic block copolymer. G.D. acknowledges French National Research Agency for funding (project NanophosforLED, ANR-17-CE09-0035-01). Additional support came from the Spanish Ministry of Economy and Competitiveness project MAT2016-75362-C3-1-R, the Spanish Ministry of Sciences, Innovation and Universities project PID2019-106211RB-I00, by the Instituto de Salud Carlos III (PI16/00812 and PI19/00565), through the Comunidad Autónoma de Madrid (B2017/BMD-3867RENIMCM) and co-financed by the European Structural and investment fund. Additional funding was provided by the European Union's Horizon 2020 FET Open project NanoTBTech (grant agreement 801305), the Fundación para la Investigación Biomédica del Hospital Universitario Ramón y Cajal project IMP18_38(2018/0265), and also COST action CA17140. J. Y. acknowledges a scholarship from the China Scholarship Council (No. 201704910867), and D. H. O. is thankful to the Instituto de Salud Carlos III for a Sara Borrell Fellowship (CD17/00210).

REFERENCES

[1] McKinnon, K.M. "Flow Cytometry: An Overview", *Curr Protoc Immunol.* **2019**, 120: 5.1.1-5.1.11

[2] Tipirneni, K.E.; Rosenthal, E.L.; Moore, L.S.; Haskins, A.D.; Udayakumar, N.; Jani, A.H.; Carroll, W.R.; Morlandt, A.B.; Bogyo, M.; Rao, J.; Warram, J.M. "Fluorescence Imaging for Cancer Screening and Surveillance" *Mol Imaging Biol.* **2017**, 19(5), 645-655

[3] Nagaya, T.; Nakamura, Y.A.; Choyke, P.L.; Kobayashi, H. "Fluorescence-Guided Surgery" *Frontiers in Oncology* **2017**, 7, 314

[4] Van Dam, G.M.; Themelis, G.; Crane, L.M.A.; Harlaar, N.J.; Pleijhuis, R.G.; Kelder, W.; Sarantopoulos, A.; de Jong, J. S.; Arts, H.J.G.; van der Zee, A.G.J.; Bart, J.; Low, P.S.; Ntziachristos, V. "Intraoperative tumor-specific fluorescence imaging in ovarian cancer by folate receptor-α targeting: first in-human results" *Nature Medicine*, **2011**, 17, 1315-1319.

[5] Herranz, M.; Ruibal A. "Optical imaging in breast cancer diagnosis: the next evolution", *J Oncol.* **2012**, 863747.

[6] Wang, J.; Zhang, G.; Li, Q.; Jiang, H.; Liu, C.; Amatore, C.; Wang, X. "*In vivo* self-bio-imaging of tumors through in situ biosynthesized fluorescent gold nanoclusters" *Sc. Reports* **2013**, 3, 1157

[7] Jain, A.; Fournier, P.G. J.; Mendoza-Lavaniegos, V.; Sengar, P.; Guerra-Olvera, F.M.; Iñiguez, E.; Kretzschmar, T.G.; Hirata, G. A.; Juárez, P. "Functionalized rare earth-doped nanoparticles for breast cancer nanodiagnostic using fluorescence and CT imaging" *J Nanobiotechnol* **2018**, 16, 26

[8] Hemmer, E.; Benayas, A.; Légaré, F.; Vetrone, F. "Exploiting the Biological Windows: Current Perspectives on Fluorescent Bioprobes Emitting above 1000 nm" *Nanoscale Horiz*. **2016**, 1, 168-184.

[9] Kim, K.H.; Singha, S.; Woong Jun, Y.; Reo, Y.J.; Kim, H.R.; Ryu, H.G.; Bhunai, S.; Ahn, K.H. "Far-red/near-infrared emitting, two-photon absorbing, and bio-stable amino-Si-pyronin dyes" *Chem. Sci.* **2019**, 10, 9028-9037.

[10] Haque, A.; Faizi, M.S.H.; Rather, J.A.; Khan, M.S. "Next generation NIR fluorophores for tumor imaging and fluorescence-guided surgery: A review" *Bioorganic & Medicinal Chemistry* **2017**, 25, 2017-2034.

[11] Jenkins, R.; Burdette, M.K.; Foulger, S.H. "Mini-review: fluorescence imaging in cancer cells using dye-doped nanoparticles" *RSC Adv*. **2016**, 6, 65459-65474.

[12] Li, Z.; Sun, Q.; Zhu, Y.; Tan, B.; Xu, Z.P.; Dou, S.X. "Ultra-small Fluorescent Inorganic Nanoparticles for Bioimaging" *J. Mater. Chem. B* **2014**, 2, 2793-2818.

[13] Gao, J.; Chen, X.; Cheng, Z. "Near-Infrared Quantum Dots as Optical Probes for Tumor Imaging" *Curr Top Med Chem.* **2010**, 10(12), 1147-1157.

[14] Liu, P.; Mu, X.; Zhang, X.-D.; Ming, D. "The Near-Infrared-II Fluorophores and Advanced Microscopy Technologies Development and Application in Bioimaging" *Bioconjugate Chem.* **2020**, 31, 260-275.

[15] Hong, G.; Lee, J.C.; Robinson, J.T.; Raaz, U.; Xie, L.; Huang, N.F.; Cooke, J.P.; Dai, H. "Multifunctional *in vivo* vascular imaging using near-infrared II fluorescence" *Nat Med.* **2012**, 18(12), 1841-1846

[16] Del Rosal, B.; Benayas, A. "Strategies to Overcome Autofluorescence in Nanoprobe-Driven In Vivo Fluorescence Imaging" *Small Methods*, **2018,** 2, 1800075.

[17] Ortgies, D.H.; Rodriguez, E.M. "Near Infrared-Emitting Bioprobes for low autofluorescence Imaging Techniques" Chapter 9 from Book "Near Infrared-Emitting Nanoparticles for Biomedical Applications" Ed. By A. Benayas, E. Hemmer, G. Hong, D. Jaque, Springer, Switzerland, **2020**

[18] Skripka, A.; Morinvil, A.; Matulionyte, M.; Cheng, T.; Vetrone, F. "Advancing Neodymium Single-Band Nanothermometry" *Nanoscale* **2019**, 11, 11322-11330.

[19] Suta, M.; Antić, Ž.; Đorđević, V.; Kuzman, S.; Dramićanin, M.D.; Meijerink, A. "Making Nd^{3+} a Sensitive Luminescent Thermometer for Physiological Temperatures—An Account of Pitfalls in Boltzmann Thermometry" *Nanomaterials* 2020, 10(3), 543.

[20] Villa, I.; Vedda, A.; Cantarelli, I. X.; Pedroni, M.; Piccinelli, F.; Bettinelli, M.; Speghini, A.; Quintanilla, M.; Vetrone, F.; Rocha, U.; Jacinto, C.; Carrasco, E.; Rodriguez, F.; Juarranz, A.; del Rosal, B.; Ortgies, D.; Gonzalez, P.; Sole Garcia, J.; Jaque, D. "1.3 μm Emitting SrF_2:Nd^{3+} Nanoparticles for High Contrast In Vivo Imaging in the Second Biological Window" *Nano Res.* **2015**, 8(2), 649-665.

[21] Rocha, U.; Jacinto da Silva, C.; Ferreira Silva, W.; Guedes, I.; Benayas, A.; Martinez Maestro, L.; Acosta Elias, M.; Bovero, E.; van Veggel, F.C.J.M.; Garcia Sole, J.A.; Jaque, D. "Subtissue Thermal Sensing Based on Neodymium-Doped LaF3 Nanoparticles" *ACS Nano* **2013**, 7(2), 1188-1199.

[22] Chen, G.; Ohulchanskyy, T.Y.; Liu, S.; Law, W.-C.; Wu, F.; Swihart, M.T.; Agren, H.; Prasad, P.N. "Core/Shell $NaGdF_4$:Nd^{3+}/$NaGdF_4$ Nanocrystals with Efficient Near-Infrared to Near-Infrared Downconversion Photoluminescence for Bioimaging Applications" *ACS Nano* **2012**, 6(4), 2969-2977.

[23] Yu, Z.F.; Shi, J.P.; Li, J.L.; Li, P.H.; Zhang H.W. "Luminescence enhancement of CaF_2:Nd^{3+} nanoparticles in the second near-infrared window for in vivo imaging through Y^{3+} doping" J. *Mater. Chem. B* **2018**, 6, 1238-1243.

[24] Feng, Y.; Xiao, Q.; Zhang, Y.; Li, F.; Li, Y.; Li, C.; Wang, Q.; Shi, L.; Lin, H. "Neodymium-doped $NaHoF_4$ nanoparticles as near-infrared luminescent/T_2-weighted MR dual-modal imaging agents in vivo" *J. Mater. Chem. B* **2017**, 5, 504-510.

[25] Del Rosal, B.; Pérez-Delgado, A.; Misiak, M.; Bednarkiewicz, A.; Vanetsev, A.S.; Orlovskii, Y.; Jovanović, D.J.; Dramićanin, M.D.; Rocha, U.; Kumar, K.U.; Jacinto, C.; Navarro, E.; Rodríguez, E.M.; Pedroni, M.; Speghini, A.; Hirata, G.A.; Martín, I.R.; Jaque, D. "Neodymium-doped nanoparticles for infrared fluorescence bioimaging: The role of the host" *J. Appl. Physics* **2015**, 118, 143104.

[26] Dantelle, G.; Testemale, D.; Homeyer, E.; Cantarano, A.; Kodjikian, S.; Dujardin, C.; Hazemann, J.L.; Ibanez, A. "A new solvothermal method for the synthesis of size-controlled YAG:Ce single-nanocrystals" *RSC Adv.* **2018**, 8, 26857-26870.

[27] Cantarano, A.; Testemale, D.; Sousa Nobre, S.; Potdevin, A.; Bruyère, R.; Barbara, A.; Hazemann, J.-L.; Ibanez, A.; Dantelle, G. "Twofold advantage of gas bubbling for the advanced solvothermal preparation of efficient YAG:Ce nanophosphors preparation" *J. Mat. Chem. C* **2020**, 8, 9382-9390.

[28] Dantelle, G.; Matulionyte, M.; Testemale, D.; Cantarano, A.; Ibanez, A.; Vetrone, F. "Nd^{3+}-doped $Gd_3Sc_2Al_3O_{12}$ nanocrystals: towards efficient nanoprobes for temperature sensing" *Phys. Chem. Chem. Phys.* **2019**, 21, 11132-11141.

[29] Benayas, A.; del Rosal, B.; Pérez-Delgado, A.; Santacruz-Gómez, K.; Jaque, D.; Hirata, G.A.; Vetrone, F. "Nd:YAG Near-Infrared Luminescent Nanothermometers" *Adv. Optical Mater.* **2015**, 3(5), 687-694.

[30] Kasuya, R.; Isobe, T.; Kuma, H.; Katano, J. "Photoluminescence Enhancement of PEG-Modified YAG:Ce^{3+}Nanocrystal Phosphor Prepared by Glycothermal Method" *J. Phys. Chem. B* **2005**, 109 (47), 22126-22130.

[31] Asakura, R.; Isobe, T.; Kurokawa, K.; Aizawa, H.; Ohkubo, M. "Tagging of avidin immobilized beads with biotinylated YAG:Ce^{3+} nanocrystal phosphor" *Anal Bioanal Chem.* **2006**, 386, 1641-1647.

[32] Dong, B.; Wang, J.; Sun, J.; Xu, S.; Bai, X.; Jiang, Z.; Xia, L.; Sun, L.; Song, H. "Non-photobleaching YAG:Ce nanoparticles for optical imaging with blue excitation" *RSC Advances* **2012**, 2, 3897-3905.

[33] Sengar, P.; Juárez, P.; Verdugo-Meza, A.; Arellano, D.L.; Jain, A.; Chauhan, K.; Hirata, G.A.; Fournier, P.G.J. "Development of a functionalized UV-emitting nanocomposite for the treatment of cancer using indirect photodynamic therapy" *J Nanobiotechnol.* **2018**, 16, 19.

[34] Gérardin, C.; Sanson, N.; Bouyer, F.; Fajula, F.; Putaux, J.-L.; Joanicot, M.; Chopin, T. "Highly Stable Metal Hydrous Oxide Colloids by Inorganic Polycondensation in Suspension" *Angewandte Chemie Int. Ed.* **2003**, 42, 3681-3685.

[35] Bouyer, F.; Sanson, N.; Destarac, M.; Gérardin, C. "Hydrophilic block copolymer-directed growth of lanthanum hydroxide nanoparticles" *New J. Chem.* **2006**, 30, 399-408.

[36] Layrac, G.; Destarac, M.; Gerardin, C.; Tichit, D. "Highly Stable Layered Double Hydroxide Colloids: A Direct Aqueous Synthesis Route from Hybrid Polyion Complex Micelles" *Langmuir* **2014**, 30 (32) 9663-9671.

[37] Layrac, G.; Harrisson, S.; Destarac, M.; Gérardin, C.; Tichit, D. "Synthesis of Cu-Al layered double hydroxide: Mechanism of formation and preparation of stable colloids", *Applied Clay Science* **2020**, 193, 105673

[38] Tarasov, K.; Houssein, D.; Destarac, M.; Marcotte, N.; Gérardin, C.; Tichit, D. "Stable aqueous colloids of ZnS quantum dots prepared using double hydrophilic block copolymers" *New J. Chem.* **2013**, 37, 508-514.

[39] Devoisselle, J.M.; Begu, S.; Bertorelle, F. ; Gerardin, C. ; Drogoz, A. "Vaccine composition including hybrid nanoparticles of aluminum and a water-soluble copolymer" Patent WO2013104873A1 **2013**

[40] Boudier, A.; Aubert-Pouessel, A.; Louis-Plence, P.; Gérardin, C.; Jorgensen, C.; Devoisselle, J.M.; Bégu, S. "The control of dendritic cell maturation by pH sensitive polyion complex micelles", *Biomaterials* **2009**, 30, 233-241.

[41] Testemale, D.; Argoud, R.; Geaymond, O.; Hazemann, J.-L. "High pressure/high temperature cell for X-ray absorption and scattering techniques" *Rev. Sci. Instrum.* **2005**, 76, 043905.

[42] Lupei, V.; Lupei, A.; Georgescu, S.; Diaconescu, B.; Taira, T.; Sato, Y.; Kurimura, S.; Ikesue, A. "High-resolution spectroscopy and emission decay in concentrated Nd:YAG ceramics" *Opt. Soc. Am. B* **2002** 19, 360-368.

[43] Zhang, X.; He, W.; Yue, Y.; Zhang, Y. "Influence of neodymium-doping on structure and properties of yttrium aluminum garnet" *CrystEngComm* **2013**,15, 8029-8035.

[44] Layrac, G.; Gérardin, C.; Tichit, D.; Harrisson, S.; Destarac, M. "Hybrid polyion complex micelles from poly(vinylphosphonic acid)-based double hydrophilic block copolymers and divalent transition metal ions" *Polymer* **2015**, 72, 292-300.

[45] Asakura, R.; Isobe, T.; Kurokawa, K.; Takagi, T.; Aizawa, H.; Ohkubo, M. "Effects of citric acid additive on photoluminescence properties of YAG:Ce^{3+} nanoparticles synthesized by glycothermal reaction" *J. Lum.* **2007**, 127, 416-422.

[46] Sanson, N.; Bouyer, F.; Gérardin, C.; In, M. "Nanoassemblies formed from hydrophilic block copolymers and multivalent ions" *Phys. Chem. Chem. Phys.* **2004**, 6, 1463-1466.

[47] Sanson, N.; Bouyer, F.; Destarac, M.; In, M.; Gérardin, C. "Hybrid Polyion Complex Micelles Formed from Double Hydrophilic Block Copolymers and Multivalent Metal Ions: size control and nanostructure" *Langmuir* **2012**, 28, 3773-3782.

[48] Sanson, N.; Putaux, J.-L.; Destarac, M.; Gérardin, C.; Fajula, F. "Hybrid organic-inorganic colloids with a core-corona structure: a transmission electron microscopy investigation" *Macromolecular Symposia* **2005**, 226, 279-288.

[49] He, X.; Liu, X.; Li, R.; Yang, B.; Yu, K.; Zeng, M.; Yu, R. "Effects of local structure of Ce^{3+} ions on luminescent properties of $Y_3Al_5O_{12}$:Ce nanoparticles" *Scientific reports* 2016, **6**, 22238.

[50] Bashir, S.; Teo, Y.Y.; Naeem, S.; Ramesh, S.; Ramesh, K. "pH responsive N-succinyl chitosan/Poly(acrylamide-co-acrylic acid) hydrogels and *in vitro* release of 5-fluorouracil" *PLoS One* **2017**, 12(7): e0179250.

[51] Coates, J. "Interpretation of infrared spectra", Ed. Wiley and Son, Chichester, **2000**

[52] Hreniak, D.; Strek, W.; Mazur, P. "Preparation, spectroscopy and morphology of Nd:YAG nanostructures" *Mater. Sc.* **2002**, 20(2), 39-45.

[53] Iparraguirre, I.; Azkargorta, J.; Balda, R.; Venkata Krishnaiah, K.; Jayasankar, C.K.; Al-Saleh, M.; Fernández, J. "Spontaneous and stimulated emission spectroscopy of a Nd^{3+}-doped phosphate glass under wavelength selective pumping" *Opt. Express* **2011**, 19(20), 19442-19453.

[54] Pokhrel, M.; Ray, N.; Kumar, G.A.; Sardar, D.K. "Comparative studies of the spectroscopic properties of Nd^{3+}: YAG nanocrystals, transparent ceramic and single crystal" *Optical Materials Express 2012*, 2(3), 235-249.

[55] Boyer, J.-C.; Manseau, M.P.; Murray, J.I.; van Veggel, F.C.J.M. "Surface modification of upconverting $NaYF_4$ nanoparticles with PEG-phosphate ligands for NIR (800 nm) biolabeling within the biological window" *Langmuir* **2009**, 26, 1157-1164.

[56] Arppe, R.; Hyppänen, I.; Perälä, N.; Peltomaa, R.; Kaiser, M.; Würth, C.; Christ, S.; Resch-Genger, U.; Schäferling, M.; Soukka, T. "Quenching of the upconversion luminescence of NaYF4:Yb3+,Er3+ and NaYF4:Yb3+,Tm3+ nanophosphors by water: the role of the sensitizer Yb3+ in non-radiative relaxation" *Nanoscale*, **2015**, 7, 11746-11757.

[57] Caponetti, E.; Saladino, M.L.; Chillura Martino, D.; Pedone, L.; Enzo, S.; Russu, S.; Bettinelli, M.; Speghini, A. "Luminescence properties of neodymium-doped yttrium aluminium garnet obtained by the co-precipitation method combined with the mechanical process" *Solid State Phenom.* **2005**, 106, 7-16.

[58] Koppel, D.E. "Analysis of Macromolecular Polydispersity in Intensity Correlation Spectroscopy: The Method of Cumulants" *J. Chem. Phys.* 1972, 57, 4814.

[59] del Rosal, B.; Villa, I.; Jaque, D.; Sanz-Rodríguez, F. "*In vivo* autofluorescence in the biological windows: the role of pigmentation" *J. Biophotonics* **2016**, 9, 1059-1067.

[60] Martínez Maestro, L.; Haro-González, P.; del Rosal, B.; Ramiro, J.; Caamaño, A.J.; Carrasco, E.; Juarranz, A.; Sanz-Rodríguez, F.; García Sole, J.; Jaque, D. "Heating efficiency of multi-walled carbon nanotubes in the first and second biological windows" *Nanoscale* **2013**, 5, 7882-7889.

[61] Lifante, J.; del Rosal, B.; Chaves-Coira, I.; Fernández, N.; Jaque, D.; Ximendes, E. "The near-infrared autofluorescence fingerprint of the brain", *J. Biophotonics* **2020**, DOI: 10.1002/jbio.202000154

[62] Wawrzynczyk, D.; Bednarkiewicz, A.; Nyk, M.; Strek, W.; Samoc, M. "Neodymium(iii) doped fluoride nanoparticles as non-contact optical temperature sensors" *Nanoscale* **2012**, 4, 6959-6961.

[63] Balabhadra, S.; Debasu, M.L.; Brites, C.D.S.; Rocha, J.; Carlos, L.D. "Implementing luminescence thermometry at 1.3 μm using $(GdNd)_2O_3$ nanoparticles" *J. Lum.* **2016**, 180, 25-30.

[64] Kolesnikov, I.E.; Kalinichev, A.A.; Kurochkin, M.A.; Mamonova, D.V.; Kolesnikov, E.Y.; Lähderanta, E.; Mikhailov, M.D. "Bifunctional heater-thermometer Nd^{3+}-doped nanoparticles with multiple temperature sensing parameters" *Nanothechnology* **2019**, 30 145501

[65] Pedroni, M.; Cortelletti, P.; Cantarelli, I.X.; Pinna, N.; Canton, P.; Quintanilla, M.; Vetrone, F.; Speghini, A. "Colloidal nanothermometers based on neodymium doped alkaline-earth fluorides in the first and second biological windows" *Sensors and Actuators B: Chemical* **2017**, 250, 147-155.

[66] Collins, S.F.; Baxter, G.W.; Wade, S.A. "Comparison of fluorescence-based temperature sensor schemes: Theoretical analysis and experimental validation" *J. Applied Physics* **1998**, 84, 4649

[67] Huang, P.; Zheng, W.; Tu, D.; Shang, X.; Zhang, M.; Li, R.; Xu, J. ; Liu, Y. ; Chen, X. "Unraveling the Electronic Structures of Neodymium in $LiLuF_4$ Nanocrystals for Ratiometric Temperature Sensing" *Adv. Sci.* **2019**, 6, 1802282.

[68] Bednarkiewicz, A.; Marciniak, L.; Carlos, L.D.; Jaque, D. "Standardizing luminescence nanothermometry for biomedical applications" *Nanoscale* **2020**,12, 14405-14421.

[69] Xi, Y.; Chang, Z.; Ye, X.; Huang, H.; Huang, Y.; Xiao, Q.; Lin, H. "Ultra-small Nd^{3+}-doped nanoparticles as nearinfrared luminescent biolabels of hemin in bacteria" *Nanoscale* **2016**, 8, 1288-1292.

[70] Ximendes, E.C.; Queiroz Santos,W.; Rocha, U.; Kagola, U.K.; Sanz-Rodríguez, F.; Fernández, N.; da Silva Gouveia-Neto, A.; Bravo, D.; Martín Domingo, A.; del Rosal, B.; Brites, C.D.S.; Carlos, L.D.; Jaque, D.; C. Jacinto "Unveiling in Vivo Subcutaneous Thermal Dynamics by Infrared Luminescent Nanothermometers" *Nano Lett*. **2016**, 16, 3, 1695–1703.

[71] Xi, J.; Ding, M.; Dai, J.; Pan, Y.; Chen, D.; Ji, Z. "Comparison of upconversion luminescent properties and temperature sensing behaviors of β-$NaYF_4$:Yb^{3+}/Er^{3+} nano/microcrystals prepared by various synthetic methods" *J. Mat. Sc. Materials in Electronics* **2016**, 27, 8254-8270.

[72] Dong, B.; Hu, R.N.; Cao, B.S.; Li, Z.P.; He, Y.Y.; Zhang, Z.Y.; Wolfbeis, O.S. "Size dependence of the upconverted luminescence of $NaYF_4$:Er,Yb microspheres for use in ratiometric thermometry" *Phys. Chem. Chem. Phys.* **2014**,16, 20009-20012.

[73] Dong, D.; Qiyue, L.; Yan, S.; Jiang, D.J. "Thermal sensitivity and stability of $NaYF_4$:Yb^{3+}, Er^{3+} upconversion nanowires, nanorods and nanoplates" *Materials Letters* **2013**, 110, 233-236.

[74] Wang, X.; Kong, X.; Yu, Y.; Sun, Y.; Zhang, H. "Effect of Annealing on Upconversion Luminescence of ZnO:Er^{3+} Nanocrystals and High Thermal Sensitivity" *J. Phys. Chem. C* **2007**, 111, 15119-15124.

[75] Warnant, J.; Reboul, J.; Aqil, A.; Cacciaguerra, T.; Jerome, C.; Gerardin, C. "Nanostructured silica templated by double hydrophilic block copolymers with acomb-like architecture" *Powder Technology* **2011**, 208, 461-466.

[76] del Rosal, B.; Ortgies, D.H.; Fernández, N.; Sanz-Rodríguez, F.; Jaque, D.; Martín Rodríguez, E. "Overcoming Autofluorescence: Long-Lifetime Infrared Nanoparticles for Time-Gated In Vivo Imaging" *Adv. Mater.* **2016,** 28, 10188-10193.

[77] Tan, M.; del Rosal, B.; Zhang, Y.; Martín Rodríguez, E.; Hu, J.; Zhou, Z.; Fan, R.; Ortgies, D.H.; Fernández, N.; Chaves-Coira, I.; Núñez, Á.; Jaque, D.; Chen, G. "Rare-earth-doped fluoride nanoparticles with engineered long luminescence lifetime for time-gated in vivo optical imaging in the second biological window" *Nanoscale* **2018**, 10, 17771-17780.

[78] Petera, S.; Patela, A.; Kitai, A. "Photoluminescence enhancement of Ce:YAG nanophosphors via doped/ T intrinsic core/shell structures" *J. Lumin.* **2019**, 211, 82–87.

BRIEFS

Stabilization of well-crystallized YAG:Nd^{3+} nanocrystals by a double hydrophilic block copolymer allows for the achievement of stable aqueous colloidal solutions used for autofluorescence-free *in vivo* readout.
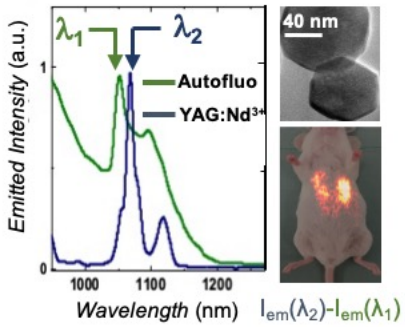
TOC